Propagation modeling of ocean-scattered low-elevation GPS signals for maritime tropospheric duct inversion*

Zhang Jin-Peng(张金鹏)[a], Wu Zhen-Sen(吴振森)[a]†, Zhao Zhen-Wei(赵振维)[b], Zhang Yu-Sheng(张玉生)[b], and Wang Bo(王 波)[c]

[a] *School of Science, Xidian University, Xi'an* 710071, *China*

[b] *China Research Institute of Radio Wave Propagation, Qingdao* 266107, *China*

[c] *Institute of Oceanographic Instrumentation, Qingdao* 266001, *China*

(Received 28 February 2012; revised manuscript received 14 May 2012)

The maritime tropospheric duct is a low-altitude anomalous refractivity structure over the ocean surface, and it can significantly affect the performance of many shore-based/shipboard radar and communication systems. We propose the idea that maritime tropospheric ducts can be retrieved from ocean forward-scattered low-elevation global positioning system (GPS) signals. Retrieval is accomplished by matching the measured power patterns of the signals to those predicted by the forward propagation model as a function of the modified refractivity profile. On the basis of a parabolic equation method and bistatic radar equation, we develop such a forward model for computing the trapped propagation characteristics of an ocean forward-scattered GPS signal within a tropospheric duct. A new GPS scattering initial field is defined for this model to start the propagation modeling. A preliminary test on the performance of this model is conducted using measured data obtained from a 2009-experiment in the South China Sea. Results demonstrate that this model can predict GPS propagation characteristics within maritime tropospheric ducts and serve as a forward model for duct inversion.

Keywords: global positioning system, ocean surface scattering, propagation modeling, tropospheric duct inversion

PACS: 92.60.Cc, 41.20.Jb **DOI:** 10.1088/1674-1056/21/10/109202

1. Introduction

A tropospheric duct is a low-altitude anomalous refractivity structure that often occurs above the ocean and land surfaces.[1,2] Radio waves with appropriate frequencies and launching angles can be trapped by tropospheric ducts and are propagated to beyond line-of-sight distances, resulting in over-the-horizon detection. However, these ducts can also lead to a radar hole and induce target tracking failure because of the reduction in the amount of energy that reaches the region immediately above or below the ducts. Therefore, the forecast or inversion of tropospheric ducts is important for the performance predictions of many radar and communication systems.

Various methods and devices have been used for refractivity estimation (i.e., tropospheric duct inversion); these include *in situ* meteorological measurements via radiosondes or rocketsondes,[3] microwave refractometers,[4] and many numerical weather prediction models.[5] A recently proposed promising approach to the remote sensing of lower atmospheric refractivity profiles is refractivity from clutter (RFC), which performs refractivity estimation by matching radar-received clutter against that modeled using the parabolic wave equation (PWE) theory.[6,7] Among the advantages of this approach are low costs, convenient implementation, and temporal and spatial tracking of refractivity profiles in a dynamically changing environment. Rogers *et al.*[8] employed the RFC technique to estimate the evaporation duct from radar sea clutter observations using a nonlinear least-squares inversion procedure. Gerstoft *et al.*[9] and Yardim *et al.*[10] employed this technique to estimate the refractivity profiles of maritime surface-based ducts. Recently, Huang *et al.*,[11] Zhao *et al.*,[12] Sheng and Huang[13] did much work on the refractivity estimation, including RFC inversions, ray tracing/correlation estimations,[14] and angle-of-arrival estimations.[15] A good review of many other RFC applications can be found in Ref. [16].

In recent years, global positioning system (GPS)

*Project supported by the National Natural Science Foundation of China (Grant Nos. 61172031 and 41175012).

†Corresponding author. E-mail: wuzhs@mail.xidian.edu.cn

© 2012 Chinese Physical Society and IOP Publishing Ltd

signals have become an attractive tool for ocean/land surface and atmospheric remote sensing. Compared with remote sensing by actively transmitted radar signals, this approach is a passive technique that presents several advantages: (i) A GPS signal is passively transmitted at all times and in all weather conditions; it is also freely available to all users. (ii) This technique does not require dedicated transmitters for the active radar remote sensing systems, thereby reducing instrument costs. (iii) Multiple samples of GPS signals can be received from GPS satellites at different elevations and azimuths, which carry different environmental information conducible to remote sensing. Ocean-reflected or scattered GPS signals were first used by Martín-Neira[17] in developing a bistatic ocean altimetry system. Later, Garrison *et al.*[18] recognized that this type of signal could be used as a new oceanographic remote sensing tool, given that it carries abundant information about propagation paths and ocean surface conditions. Since then, more researchers have become enthusiastic about the potential applications of GPS signals in ocean altimetry,[19] sea state determination,[20] and remote sensing of ocean wind speed.[21,22]

GPS signals have been successfully used in inferring atmospheric refractivity profiles. Anderson[23] used a direct inference technique to predict the refractivity profiles from low-elevation angle measurements of GPS signals. However, this technique achieves only moderate success because of the limitations presented by path-induced random range/elevation angle errors. Lowry *et al.*[24] estimated the refractivity structure from the measured GPS tropospheric delays, but the height of the estimated refractivity profile was in the order of several kilometers, making it unsuitable for describing a low-altitude tropospheric duct, much less a maritime evaporation duct. Because tropospheric ducts can heavily affect or trap the GPS signals scattered from the ocean surface at low grazing angles (to be analysed in Section 2), information about these ducts may be carried by the GPS signals propagating along long-range paths above the ocean surface. In this respect, these signals can be used to retrieve the tropospheric ducts occurring on maritime propagation paths. Unlike the GPS applications described in the preceding paragraph, in which the employed GPS signals usually come from high-elevation and nearly specular reflections, ocean-scattered GPS signals from a low-elevation satellite are preferable for tropospheric duct retrieval because more energy can be scattered at low grazing angles when the GPS incident angle is large and more scattered rays (more energy) can be affected or trapped by the duct, which is beneficial to the retrieval process.

In this paper, we propose that maritime tropospheric ducts can be retrieved from ocean forward-scattered low-elevation GPS signals. The conceived primary method for this retrieval is to match the measured power patterns of the ocean forward-scattered GPS signals to those predicted by the forward propagation model. This paper focuses primarily on the development of a forward model to provide a basis for performing the retrieval work mentioned above. Using the PWE technique and bistatic radar equation theory as bases, we develop a forward propagation model that associates the received power of an ocean forward-scattered GPS signal with the modified refractivity profile of a tropospheric duct. In this model, the GPS PWE works with a newly developed initial field to start the propagation modeling. A preliminary test on the performance of this model is conducted using the measured data obtained from a experiment conducted in 2009 in the South China Sea. Finally, the possibility of maritime tropospheric duct inversion from ocean forward-scattered low-elevation GPS signals is analysed.

2. Effect of tropospheric ducts on ocean forward-scattered GPS signals

2.1. Tropospheric duct structure

A tropospheric duct is formed by small variations in the index of refraction of the troposphere. These variations are due to the anomalous vertical gradients of temperature and humidity. Three typical types of tropospheric ducts occur over the ocean surface: evaporation, surface-based, and elevated ducts (Fig. 1).

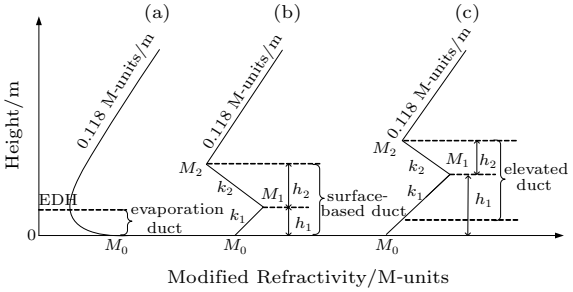


Fig. 1. Modified refractivity profiles for three typical maritime tropospheric ducts: (a) evaporation duct, (b) surface-based duct, (c) elevated duct.

The evaporation duct created by a rapid decrease in moisture immediately adjacent to the ocean surface is a nearly permanent propagation mechanism for the radar waves propagating over the ocean surface. The modified refractivity profile (M-profile) model commonly used for evaporation ducts is the log–linear Paulus–Jeske model.[25] This model is parameterized using only the evaporation duct height (EDH) as follows:

$$M(h) = M_0 + 0.125h - 0.125\delta \ln[(h + h_0)/h_0], \quad (1)$$

where h is the height (m) above the mean sea level; δ denotes the EDH (m); h is a roughness factor whose typical over-water value is 1.5×10^{-4} m; M_0 represents the modified refractivity at the sea surface, taken as 330 M-units in this paper.

Both surface-based and elevated ducts are usually formed by a rapid transition between a relatively warm, dry air mass above, and a cooler, moister air mass below. The primary difference between them is whether the duct extends down to the ocean/land surface. A four-parameter trilinear M-profile model[26] is used in this paper to parameterize the atmospheric refractivity structures of these two types of maritime tropospheric ducts. The four defining parameters are the trapping-layer base height h_1, base slope k_1, inversion-layer thickness h_2, and slope k_2. The slope of the top layer is taken as the standard refractivity gradient at 0.118 M-units/m.

2.2. Trapping capability

The propagation of ocean-scattered GPS signals in a maritime tropospheric duct environment is illustrated in Fig. 2. Two conditions are necessary for ducting propagation to occur. One is that the wavelength must be shorter than the cut-off wavelength, which is the longest wavelength that can be trapped by the duct. The other is an appropriate launching angle below a critical value, i.e., the critical trapping angle.

The maximum cut-off wavelength for a tropospheric duct can be estimated by the expression formulated by Turton *et al.*[2] as

$$\lambda_{\max} = C \int_{h_L}^{h_U} \Big[M(h) - M_U\Big]^{1/2} \mathrm{d}h, \quad (2)$$

where h_L and h_U are the lower and upper limits of the duct, respectively; h is the height above the land or ocean surface; M_U represents the modified refractivity at the top of the duct; and $M(h)$ denotes the vertical M-profile. C is a constant equal to 3.77×10^{-3} for a surface-based duct or 5.66×10^{-3} for an elevated duct.

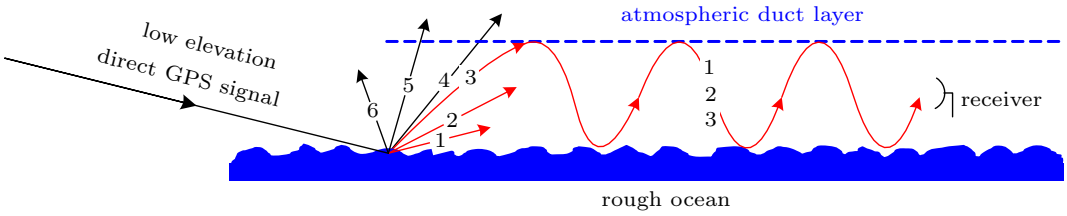


Fig. 2. (colour online) Schematic plot of the propagation of ocean-scattered GPS signals in a tropospheric duct environment.

An evaporation duct formed over the ocean surface can normally be regarded as a shallow surface-based duct. Using the M-profile model given by Eq. (1), we can express the cut-off wavelength, Eq. (2), for an evaporation duct as

$$\lambda_{\max} = 3.77\times10^{-3} \int_0^{\delta} \Big[0.125(h-\delta) + 0.125\delta \ln\frac{\delta + h_0}{h + h_0}\Big]^{1/2} \mathrm{d}h. \quad (3)$$

For both a surface-based and an elevated duct modeled by the trilinear M-profile model (Figs. 1(b) and 1(c)), the cut-off wavelength is usually given by the following simplified formula[2]

$$\lambda_{\max} = \frac{2}{3} Ct\sqrt{\Delta M}, \quad (4)$$

where t is the duct thickness (m), and ΔM is the modified refractivity difference through the inversion layer, i.e., M_1–M_2.

The cut-off wavelength for a duct indicates only a maximum wavelength, which can be well guided. Longer wavelengths are still affected, but only to a certain extent. Figure 3 shows the cut-off wavelength propagated by three typical tropospheric ducts. The wavelength is shorter than 19.032 cm (GPS L1) for an evaporation duct with a typical EDH in a range

from 0 to 40 m, indicating that GPS L1 signals cannot be well trapped by an evaporation duct. However, as illustrated in Fig. 3(b), surface-based and elevated ducts are excellent propagation mechanisms for GPS L1 signals.

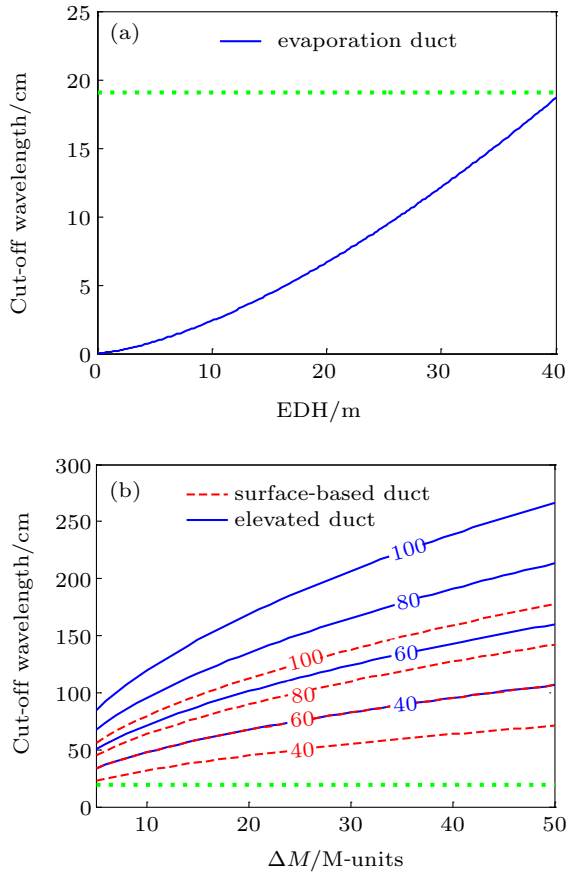


Fig. 3. (colour online) Maximum cut-off wavelength propagated by (a) an evaporation duct, (b) a surface-based duct, and an elevated duct. The number labels in panel (b) indicate the duct thickness (m). The horizontal dotted line represents the wavelength of the GPS L1 band signal (19.032 cm).

The critical trapping angle for a tropospheric duct is the corresponding launching angle when the ray travels horizontally at the duct top. It can be derived from Snell's law and simplified into

$$\theta_c \approx \sqrt{2 \times 10^{-6} \cdot (M_s - M_U)}, \quad (5)$$

where M_s and M_U denote the modified refractivity at the source height and that at the duct top, respectively.

Figure 4 shows the critical trapping angle for different increases in modified refractivity at the transmitter height compared with that at the top of a tropospheric duct. This angle is normally below 1.0°. At a larger angle, the radio waves are not sufficiently trapped. Part of the energy of the ocean forward-scattered GPS signals considered in this study can be ducted, while the remainder are steadily transmitted out of the top of the duct because the signals are distributed at a grazing angle interval [0°, 90°].

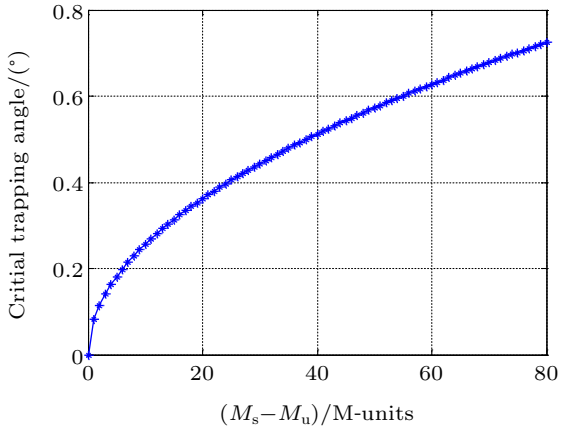


Fig. 4. (colour online) Critical trapping angle as a function of $M_s - M_U$.

To visualize the ducting effect on the ocean-scattered GPS signals, we show two height-versus-range ray tracing plots for an evaporation and surface-based duct in Fig. 5. Rays launched at low-grazing angles (below critical trapping angle θ_c) are trapped for extended ranges. Therefore, part of the energy of the GPS-scattered signals can be collected by a receiver located at an over-the-horizon position.

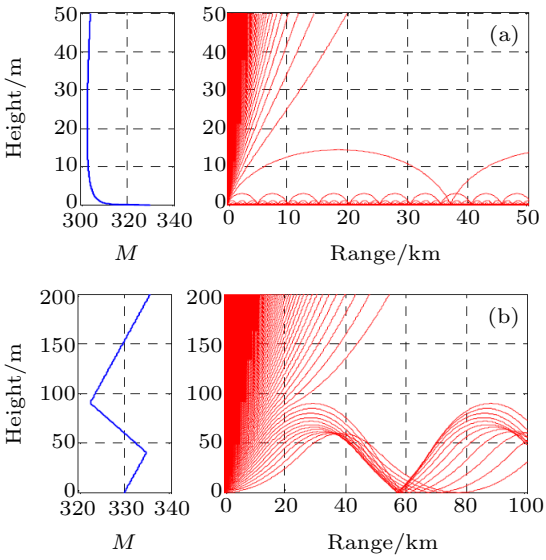


Fig. 5. (colour online) Ray tracing of the ocean forward-scattered GPS signals propagating in (a) an evaporation duct with 20-m EDH, and (b) a surface-based duct with profile parameters: $h_1 = 40$ m, $k_1 = 0.12$ M-units/m, $h_2 = 50$ m, and $k_2 = -0.243$ M-units/m. The left panels show the corresponding vertical modified refractivity profiles.

3. GPS propagation modeling

3.1. Parabolic wave equation

The PWE method is a powerful technique for predicting electromagnetic propagation in large tropospheric domains.[6,7] This method is used in this study to predict the field of the ocean forward-scattered GPS L1 signals within the maritime tropospheric duct environment.

On the assumption that all components of the field are independent of azimuth angle, the system of Maxwell's equations is reduced to a two-dimensional scalar wave equation, and the following elliptical Helmholtz equation can be obtained:

$$\left(\frac{\partial^2}{\partial x^2}+\frac{\partial^2}{\partial z^2}+k^2n^2\right)\psi(x,z)=0, \tag{6}$$

where ψ denotes the y component of either the electric or magnetic field for horizontal or vertical polarization, respectively; k is the electromagnetic wave number; and n represents the index of refraction of the atmosphere. This equation can be formally factored into two propagating terms (incoming and outgoing waves) after eliminating the rapid phase variation through reduced function $u(x,z)=\mathrm{e}^{-\mathrm{i}kx}\psi(x,z)$. Disregarding the backscattering effects yields

$$\frac{\partial u}{\partial x}+\mathrm{i}k\left(1-\sqrt{n^2+\frac{1}{k^2}\frac{\partial^2}{\partial z^2}}\right)u(x,z)=0, \tag{7}$$

which is the PWE desired for modeling the forward propagating (outgoing) waves.

Equation (7) is a pseudo-differential equation of the first order in x and can be solved by stepping techniques. It has the formal solution

$$u(x+\Delta x,z)=\exp\left[\mathrm{i}k\Delta x\left(\sqrt{n^2+\frac{1}{k^2}\frac{\partial^2}{\partial z^2}}-1\right)\right]\times u(x,z), \tag{8}$$

where Δx is the range step. Equation (8) is minimally implemented because the index of refraction n is often a function of both x and z. The refractive index effects are separated from the square root operator to enable practicable implementation. This operation can be performed by introducing an approximation of the square root operator.

The split-step solution can be obtained by a Fourier transformation. In the wide-angle case, the PWE solution in the range $x+\Delta x$ is

$$u(x+\Delta x,z)=\exp\left[\mathrm{i}k(n-1)\Delta x\right]\Im^{-1}\left\{\exp\left[\mathrm{i}k\Delta x\left(\sqrt{1-\frac{p^2}{k^2}}-1\right)\right]\Im\{u(x,z)\}\right\}, \tag{9}$$

where $\Im$ and $\Im^{-1}$ represent the forward and inverse Fourier transformations, respectively; and p is equal to $k\sin\theta$, representing the transformation variable (θ is the propagation angle in respect to the horizontal angle). This formulation is generally referred to as the split-step Fourier transform solution.

In this paper, to model the propagation over a rough, dielectric sea surface, we numerically implement the PWE using the split-step discrete mixed Fourier transform (DMFT) algorithm introduced by Dockery and Kuttler.[27] This algorithm can successfully incorporate an impedance-type boundary condition into the split-step solution.

As shown in Eq. (9), the split-step solution must start with the field on the initial vertical. The manner in which the initial fields are defined in initiating the split-step solution plays an important role in propagation prediction. The definition method for modeling the radar wave propagation is a well-developed technique; however, it cannot be used directly for the PWE propagation modeling of ocean forward-scattered GPS signals in tropospheric ducts. A new initial field definition method suitable for this case is introduced in the following section.

3.2. Initial field definition

In this subsection, the generation of a PWE initial field on the starting vertical for propagation modeling of the ocean forward-scattered GPS signals is addressed. Figure 6 shows that the PWE initial field is essentially the scattered GPS field on the vertical in the range just beyond the scattering point.

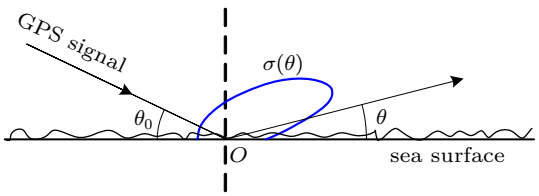


Fig. 6. Geometry of the ocean-scattered power pattern.

The source modeling has been well developed for radar wave propagation. The initial field for this

case is the radar aperture field which can be computed easily from the far-field beam pattern of the antenna using near-field/far-field transformation. We can use this transformation idea to generate the initial PWE field in the propagation modeling of the ocean forward-scattered GPS signals because the scattering point can be regarded as an equivalent transmitting antenna located at the ocean surface, and the scattering field pattern can serve as the beam pattern of the antenna. The ocean-scattering coefficient, whose angle distribution forms the scattering power pattern, can be calculated using many sophisticated methods.

The sea surface is regarded as an equivalent transmitting source; hence, this source can be assumed to be located in a free space. According to the far-field formulation given in Ref. [7] the scattered far-field $\psi^{\rm s}$ in cylindrical coordinates can be expressed by a Fourier transformation of the PWE field on the starting vertical ($x=0$) as

$$\begin{aligned}&\psi^{\rm s}(r\cos\theta, r\sin\theta)\\ \approx\ & \frac{1}{\sqrt{2\pi}}\,{\rm e}^{-{\rm i}\pi/4}\frac{\sqrt{\cos\theta}}{r}\,{\rm e}^{{\rm i}kr}\int_{-\infty}^{+\infty}u(0,z')\\ &\times{\rm e}^{-{\rm i}kz'\sin\theta}\,{\rm d}z'.\end{aligned}\tag{10}$$

Regarding the ocean scattering field pattern $\sqrt{\sigma'(\theta)}$ as the beam pattern of the antenna, we can express it in terms of the scattered field as

$$\sqrt{\sigma'(\theta)}=\lim_{r\to\infty} r\,{\rm e}^{-{\rm i}kr}\psi^{\rm s}(r\cos\theta, r\sin\theta).\tag{11}$$

By combining Eqs. (10) and (11), we have

$$\sqrt{\sigma'(\theta)}=\frac{\sqrt{\cos\theta}}{\sqrt{2\pi}}\,{\rm e}^{-{\rm i}\pi/4}\int_{-\infty}^{+\infty}u(0,z)\,{\rm e}^{-{\rm i}kz\sin\theta}\,{\rm d}z.\tag{12}$$

Applying the inverse Fourier transform, we can now obtain the PWE initial field as

$$u(0,z)=\frac{1}{\sqrt{2\pi}}\,{\rm e}^{{\rm i}\pi/4}\int_{-2\pi/\lambda}^{+2\pi/\lambda}\sqrt{\frac{\sigma'(\theta)}{\cos(\theta)}}\,{\rm e}^{{\rm i}pz}\,{\rm d}p,\tag{13}$$

where

$$\sigma'(\theta)=\begin{cases}\sigma(\theta), & \theta\geq 0,\\ 0, & \theta<0.\end{cases}\tag{14}$$

Here, $\sigma(\theta)$ represents the ocean scattering coefficient at angle θ from the horizontal; λ is the wavelength of the GPS signal. The initial field given by Eq. (13) is equivalent to the aperture field of an antenna pointing horizontally with beam pattern $\sqrt{\sigma'(\theta)}$. The only larruping characteristic of this equivalent antenna is that the maximum of the beam pattern function does not occur on the boresight.

3.3. Boundary conditions for a rough ocean surface

The PWE split-step solution is a right-hand open-boundary problem, in which two domain boundary conditions (upper and lower) are needed. The upper boundary is required to attenuate the field smoothly at a large height and propagation angle. This smooth truncation effect can be realized using the windowing method.[7] Here, we focus on the definition of the lower-boundary condition because it varies, depending on the surface type.

For the propagation modeling of the ocean forward-scattered GPS signals, the lower boundary of the PWE solution domain is the rough ocean surface. To consider its imperfectly conducting property, we use the following impedance-type boundary condition:[6]

$$\frac{\partial\psi_\phi}{\partial r}\Big|_{r=R_{\rm e}}+\alpha\psi_\phi(r=R_{\rm e})=0,\tag{15}$$

with

$$\alpha={\rm i}k\sin\theta\Big(\frac{1-\Gamma}{1+\Gamma}\Big),\tag{16}$$

where θ is the grazing angle measured from the local surface tangent; $R_{\rm e}$ is the earth's radius; ψ_ϕ represents the nonzero component of the field: either E_ϕ (H-pol) or H_ϕ (V-pol). The reflection coefficient Γ, which depends on the electrical characteristics of the surface has a specific expression for a smooth surface (i.e. the Fresnel reflection coefficient), but for a rough ocean surface, the expression should be modified to account for the amplitude reduction caused by diffuse scattering. This modification can be performed by introducing a rough surface specular reduction factor whose typical expression, given by Miller *et al.*[28] is

$$\rho_{\rm s}=\exp\Big(-\frac{1}{2}\delta^2\Big)\times{\rm I}_0\Big(\frac{1}{2}\delta^2\Big),\tag{17}$$

with

$$\delta=2kh_{\rm rms}\sin\theta,\tag{18}$$

where k is the wavenumber of the incident wave, and $h_{\rm rms}$ denotes the root-mean-square (RMS) sea wave height; δ is in essence the Rayleigh roughness parameter representing the phase difference between two rays reflected from two different areas on the surface separated by height deviation $h_{\rm rms}$; ${\rm I}_0$ is the modified Bessel function of the first kind of order zero. With this reduction factor employed, an effective specular reflection coefficient for the rough ocean surface can

be defined as $\Gamma_s = \rho_s \Gamma$.

As discussed by Dockery and Kuttler,[27] coefficient α given by Eq. (16) significantly depends on the grazing angle θ when the rough surface reflection coefficient Γ_s is used. Imposing an accurate impedance boundary condition in modeling the ocean forward-scattered GPS signal propagation within a tropospheric duct necessitates grazing angle estimation, and figure 7 shows the grazing angles of the scattered GPS signals within two surface-based ducts, estimated by a ray tracing method. The grazing angles vary rapidly with range in some range intervals, indicating that two or more propagation directions compete with each other over the ocean surface. These grazing angles should be interpolated to obtain a relatively smooth estimate because the PWE split-step implementation requires a single-valued grazing angle at each range step of the solution domain.

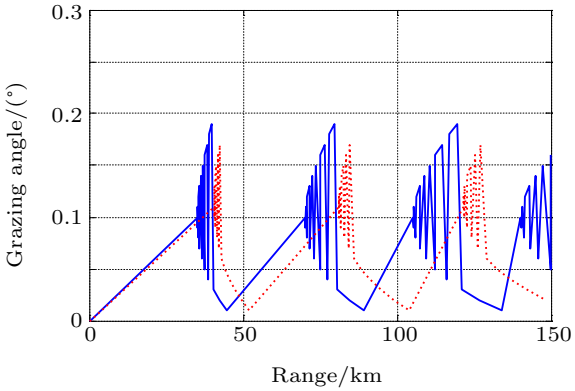


Fig. 7. (colour online) Variations of grazing angle with range for two surface-based ducts with profile parameters: (solid line) $h_1 = 15$ m, (dotted line) $h_1 = 20$ m, $k_1 = 0.12$ M-units/m, $h_2 = 30$ m, $k_2 = -0.243$ M-units/m.

4. Received GPS power pattern

4.1. Bistatic scattering system

The problem studied in the present work involving GPS scattering and propagation can be considered as a bistatic scattering system (Fig. 8), in which the GPS satellite is the transmitter, the ocean surface is the target, and the receiver is located within or above the tropospheric duct at a distance far beyond the scattering point. Before being captured by the receiver, the GPS signal suffers from three losses in space: i) path loss between the satellite and the scattering point on the ocean surface; ii) loss due to rough sea surface scattering and absorption; iii) path loss during propagating in the tropospheric duct (i.e., along path R_2). We primarily consider losses ii) and iii) in the generation of the received power pattern.

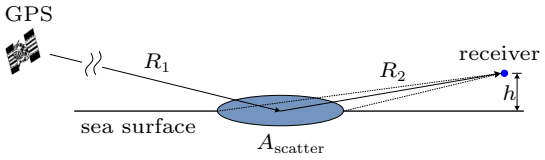


Fig. 8. (colour online) GPS bistatic scattering geometry.

Denoting the transmitted power of the GPS satellite as P_t, and the transmit antenna gain as G_t, the power density of the GPS signal arriving at the ocean surface can be expressed as

$$S_t = \frac{P_t G_t}{4\pi R_1^2} f_t^2 F_1^2, \tag{19}$$

where R_1 and F_1 are the distance and propagation factor between the transmitter and the scattering point on the ocean surface, respectively; f_t represents the pattern function of the transmitting antenna, which equals 1 in all directions for isotropic antennas. After scattering over the ocean surface and propagation within the tropospheric duct, the GPS signals at the receiving point have a power density, expressed as

$$S_r = \frac{P_t G_t}{4\pi R_1^2} f_t^2 F_1^2 \sigma_B \left(\frac{1}{4\pi R_2^2}\right) F_2^2, \tag{20}$$

with

$$\sigma_B = \sigma_B^0 A_{\text{scatter}}, \tag{21}$$

where R_2 and F_2 are the distance and propagation factor between the scattering point on the ocean surface and the GPS receiver, respectively. σ_B denotes the bistatic scattering cross section of the ocean surface, which can be expressed as the product of bistatic scattering coefficient σ_B^0 and scattering cell area A_{scatter}.

Once the power density given by Eq. (20) is determined, the received power strength can be easily obtained by multiplying it with the effective aperture of the receiving antenna. The direct GPS signal along path R_1 is assumed to travel in a free space in this study, so that the propagation factor F_1 equals 1.

4.2. Scattering coefficient

The scattering coefficient of the ocean surface, which describes the amount of power that is scattered

in a certain direction, plays an important role in determining the received power of the ducted GPS signals. Its normalized angular distribution is referred to as a "scattering power pattern", which has been used in defining the GPS PWE initial field in Subsection 3.2.

Electromagnetic scattering from the ocean surface has been extensively studied for many years, and numerous solving methods have been developed, including approximate analytical and numerical methods.[29] In the present study, the bistatic scattering coefficient of the ocean surface is calculated using a modified Kirchhoff approximation (KA) method, in which the tapered wave suggested by Thorsos[30] is applied as the incident wave to prevent the artificial edge diffraction from appearing in the case of an incident plane wave.

Considering a plane wave $\psi^{\rm inc}(\boldsymbol{r})$ incident on a rough ocean surface of height profile $z = f(x)$, the scattered field can be given by

$$\begin{aligned}\psi^{\rm s}(\boldsymbol{r}) &= \psi^{\rm total}(\boldsymbol{r}) - \psi^{\rm inc}(\boldsymbol{r}) \\ &= \int_{\rm S}\Big[\psi^{\rm total}(\boldsymbol{r}')\frac{\partial G(\boldsymbol{r},\boldsymbol{r}')}{\partial n'} \\ &\quad - G(\boldsymbol{r},\boldsymbol{r}')\frac{\partial \psi^{\rm total}(\boldsymbol{r}')}{\partial n'}\Big]{\rm d}s', \qquad (22)\end{aligned}$$

with

$$G(\boldsymbol{r},\boldsymbol{r}') = \frac{\rm i}{4}{\rm H}_0^{(1)}(k_0|\boldsymbol{r}-\boldsymbol{r}'|), \qquad (23)$$

where $\psi^{\rm total}(\boldsymbol{r})$ denotes the total field, $G(\boldsymbol{r},\boldsymbol{r}')$ is the Green's function, k_0 is the wave number in free space, and ${\rm H}_0^{(1)}$ represents the Hankel function of the first kind of order one. Equation (22) can be solved using the Kirchhoff approximation. In general, however, the rough ocean surface used in the field calculation is of a finite length, so that the errors of the field appear to be caused by the artificial truncation effect when a plane incident wave is employed in the calculation. We use the tapered wave as the incident wave to avoid this situation. The tapered wave can be expressed as follows:

$$\begin{aligned}\psi^{\rm inc}(\boldsymbol{r}) &= \exp\big\{{\rm i}k_0(x\sin\theta_{\rm i} - z\cos\theta_{\rm i})[1+w(\boldsymbol{r})]\big\} \\ &\quad \times \exp\Big[-\frac{(x+z\tan\theta_{\rm i})^2}{g^2}\Big], \qquad (24)\end{aligned}$$

with

$$w(\boldsymbol{r}) = \Big[\frac{2(x+z\tan\theta_{\rm i})^2}{g^2} - 1\Big] \Big/ (k_0 g\cos\theta_{\rm i})^2, \qquad (25)$$

where $\theta_{\rm i}$ is the incident angle and g is the tapering waist that should be sufficiently large to satisfy the wave equation. Otherwise, the ocean surface length should be larger than several correlation lengths of the surface to suppress the punctuated power at the surface edges. Using this tapered wave as the incident wave, we can obtain the scattered field under the Kirchhoff approximation from Eq. (22) as follows:

$$\psi^{\rm s}_{\rm KA}(\boldsymbol{r}) = \sqrt{\frac{\rm i}{8\pi k_0 r}}\exp({\rm i}k_0 r)\psi^{(N)}_{\rm KA}(\theta_{\rm s}), \qquad (26)$$

with

$$\begin{aligned}\psi^{(N)}_{\rm KA}(\theta_{\rm s}) &= \int_S\Big[(1+\Gamma)\psi^{\rm inc}(\boldsymbol{r}')(-{\rm i}\boldsymbol{k}_{\rm s}\cdot\hat{\boldsymbol{n}}') \\ &\quad -(1-\Gamma)\frac{\partial\psi^{\rm inc}(\boldsymbol{r}')}{\partial n'}\Big]\exp(-{\rm i}\boldsymbol{k}_{\rm s}\cdot\boldsymbol{r}'){\rm d}s', \qquad (27)\end{aligned}$$

where $\theta_{\rm s}$ is the scattering angle, and $\boldsymbol{k}_{\rm s} = k_0(\sin\theta_{\rm s}\hat{\boldsymbol{x}} + \cos\theta_{\rm s}\hat{\boldsymbol{z}})$ represents the scattering wave vector. A detailed derivation can be found in Ref. [31].

The bistatic scattering coefficient of the rough ocean surface can be defined as[32]

$$\frac{P_{\rm s}}{P_{\rm inc}} = \int_{-\pi/2}^{\pi/2}\sigma^0_{\rm B}(\theta_{\rm s}){\rm d}\theta_{\rm s}, \qquad (28)$$

where $P_{\rm inc}$ and $P_{\rm s}$ represent the total power received and scattered by the rough ocean surface, respectively. Then, it can be expressed as

$$\sigma^0_{\rm B}(\theta_{\rm s}) = \frac{\big|\psi^{(N)}_{\rm KA}(\theta_{\rm s})\big|^2}{8\pi k_0 g\sqrt{\dfrac{\pi}{2}}\cos\theta_{\rm i}\Big[1-\dfrac{1+2\tan^2\theta_{\rm i}}{2(k_0 g\cos\theta_{\rm i})^2}\Big]}. \qquad (29)$$

Three examples of the bistatic scattering coefficients of the horizontal and vertical components of the right-hand circularly polarized GPS L1 signals are shown in Fig. 9. The GPS elevation angle is equal to the complement of incident angle $\theta_{\rm i}$. The wind speed at an altitude of 19.5 m above the ocean surface is assumed to be 8 m/s. The temperature and salinity of the sea water are 20° and 30‰ respectively, which correspond to the permittivity (72.36, −53.61) of the GPS L1 band (1.5754 GHz). The peaks of the bistatic scattering coefficients for the two polarizations appear around the specular direction, which is a logical result according to Snell's law. The corresponding normalized scattering field patterns (in polar coordinates) can be derived from these scattering coefficients, and are regarded as the beam patterns of equivalent transmitting antennas in modeling the propagation of the ocean forward-scattered GPS signals.

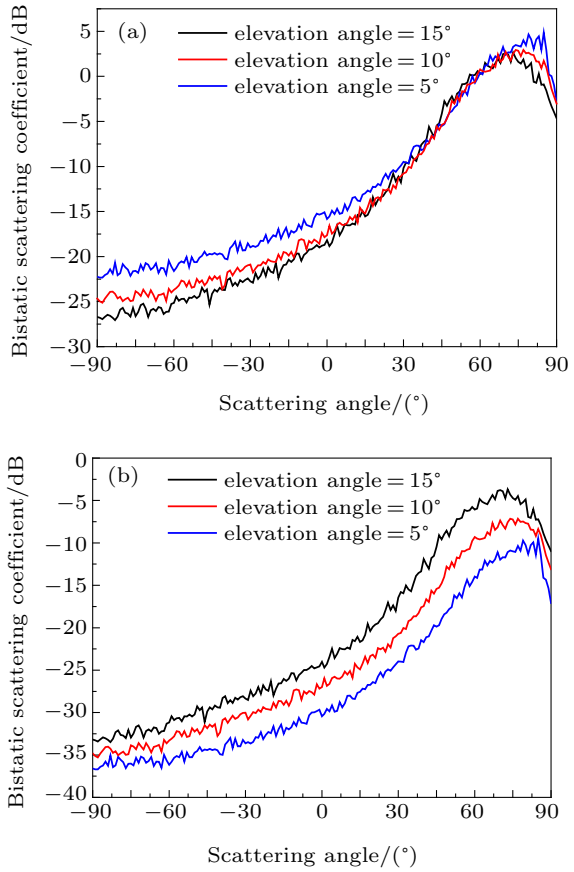


Fig. 9. (colour online) Bistatic scattering coefficients of the ocean surface for the horizontally (a) and vertically (b) polarized GPS L1 band (1.5754 GHz).

4.3. Pattern propagation factor

Propagation factor F_2 in Eq. (20) is the parameter that represents the effect of the propagation path within the tropospheric duct on the power density of the GPS signals. Substituting Eq. (21) into Eq. (20) and introducing a normalized scattering coefficient of the ocean surface yield

$$S_{\rm r} = \frac{P_{\rm t}G_{\rm t}}{4\pi R_1^2} f_{\rm t}^2 F_1^2 \Big(\frac{\sigma_{\rm B}^0}{\sigma_{\rm B\,max}^0}\Big) \times \sigma_{\rm B\,max}^0 A_{\rm scatter} \Big(\frac{1}{4\pi R_2^2}\Big) F_2^2, \quad (30)$$

where $\sigma_{\rm B\,max}^0$ denotes the maximum of the bistatic scattering coefficient. The term in the first bracket represents the normalized scattering coefficient, i.e., the scattering power pattern. The square-root of this power pattern multiplied by F_2 can be regarded as the pattern propagation factor between the equivalent transmitting antenna (ocean surface scattering) and receiving point, that is,

$$F = \sqrt{\frac{\sigma_{\rm B}^0}{\sigma_{\rm B\,max}^0}} F_2. \quad (31)$$

In physical meanings, pattern propagation factor F is defined as $F = 10\log|E/E_0|$, where E is the amplitude of the electric field at a given point within specified environments, and E_0 denotes the amplitude of the free-space electric field when the antenna is directed toward the point in question. This factor involves the effects of both the external features of the propagation path and field pattern function $\sqrt{\sigma_{\rm B}^0(\theta_{\rm s})/\sigma_{\rm B\,max}^0}$ of the equivalent transmitting antenna located on the ocean surface.

Equation (30) can be rewritten as follows:

$$S_{\rm r} = \frac{P_{\rm t}G_{\rm t}}{4\pi R_1^2} f_{\rm t}^2 F_1^2 \sigma_{\rm B\,max}^0 A_{\rm scatter} \Big(\frac{1}{4\pi R_2^2}\Big) F^2. \quad (32)$$

Here, F, instead of F_2, is calculated using the DMFT PWE method as described in Section 3.

Figure 10 shows the distribution of the pattern propagation factor F of the ocean forward-scattered GPS signals in three atmospheric refractivity environments. The GPS elevation angle is 5°. The corresponding scattering power pattern used in the PWE initial field definition is shown in Fig. 9. The electrical properties of the ocean surface and wind speed assumed in the simulation are the same as those in Fig. 9. Two conclusions can be drawn by comparing the height-range diagram for a free space (Fig. 10(a)) with those for two ducting environments (Figs. 10(b) and 10(c)). First, maritime tropospheric ducts substantially extend the region with high propagation factors, indicating that they can heavily affect the propagation characteristics of the ocean forward-scattered GPS L1 signals. Second, as shown in the low parts of Figs. 10(b) and 10(c), evaporation ducts cannot sufficiently trap scattered GPS L1 band signals, but trapping behaviour is clearly observable and a beyond-the-horizon propagation occurs in the surface-based ducts. This phenomenon is consistent with the result of the trapping capability analysis presented in Section 2. Given that the tropospheric ducts affect the propagation of the ocean-scattered GPS signals and the extent of this effect varies for different ducts, maritime tropospheric duct inversion from these signals is possible.

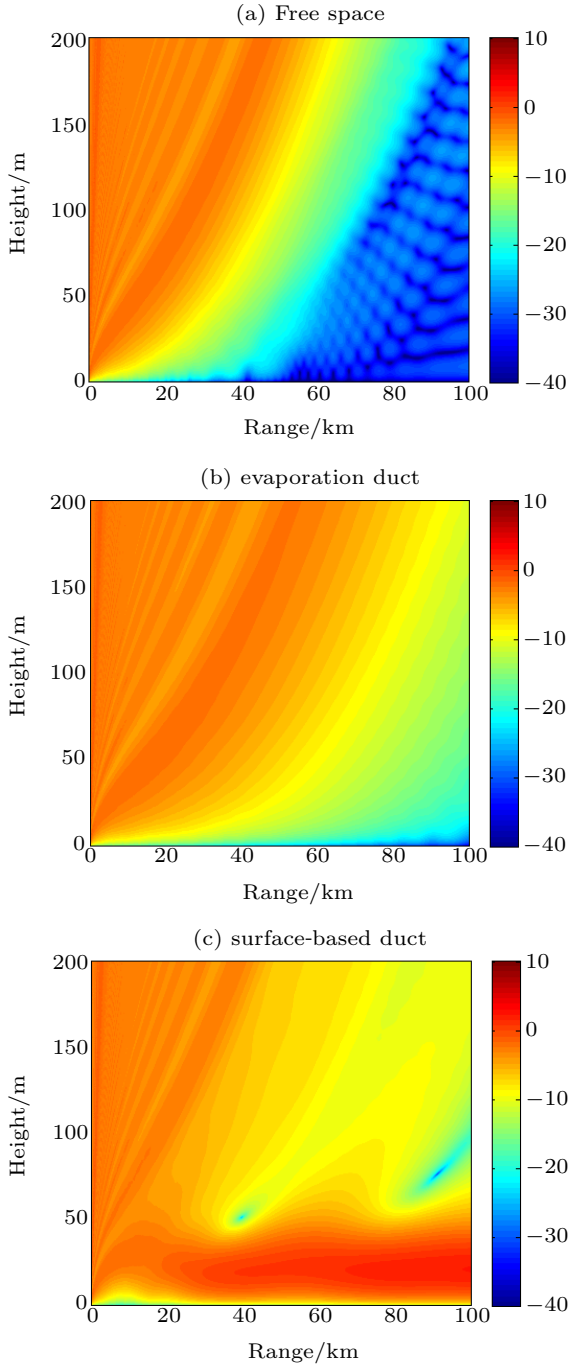


Fig. 10. (colour online) Pattern propagation factor F (in dB) between the equivalent transmitting antenna and receiving points in free space (a), an evaporation duct with an EDH of 20 m (b), and a surface-based duct with a trapping-layer base height of 20 m, a base slope of 0.12 M-units/m, an inversion-layer thickness of 30 m, and a slope of −0.243 M-units/m (c).

4.4. Numerical results

Once the power density given by Eq. (32) is known, the scattered power received by an antenna can be expressed as

$$P_{\mathrm{r}} = S_{\mathrm{r}} A_{\mathrm{e}} = \frac{\lambda^2 G_{\mathrm{r}} f_{\mathrm{r}}^2 S_{\mathrm{r}}}{4\pi}, \tag{33}$$

where λ is the wavelength; A_{e}, G_{r}, and f_{r} are the effective aperture, gain, and field pattern function of the receiving antenna, respectively.

Table 1. Parameters of the GPS receiving antenna.

Parameter	Value
Frequency/MHz	1575.42
Antenna gain/dB	30
Beamwidth/(°)	10.0
Antenna height/m, above mean sea level	8.0
Elevation angle/(°)	0.0
Polarization	LHCP
Beam pattern	Gaussian

Figure 11 shows the curves of power of the GPS scattered signals versus range R_2, received by an antenna with the parameters given in Table 1 in the three refractivity environments mentioned in the preceding section. Three GPS elevation angles are considered simultaneously to illustrate the effect of this angle on the received power strength. The tropospheric duct has a conspicuous enhancing effect on power strength. Moreover, the larger the GPS elevation angle, the lower the power strength is. This is a logical result because less energy from the ocean-scattered GPS signals can be trapped in the duct when the GPS is at a high elevation. Therefore, a lower GPS elevation angle (elev.) is preferred in tropospheric duct inversion because the receiver is of a certain sensitivity.

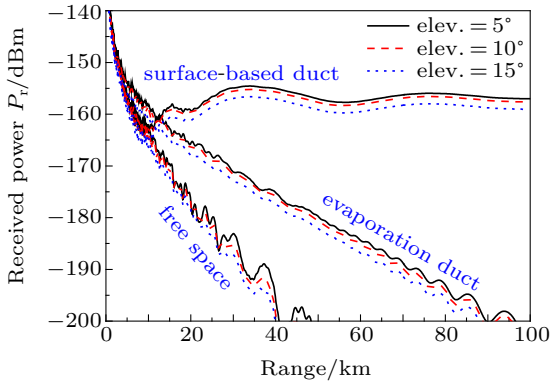


Fig. 11. (colour online) Curves of simulated GPS scattered power versus range R_2 in three different refractivity environments.

5. Comparison with experimental data

An experiment was performed in the South China Sea in June and July 2009. The core aim of the experiment was to gather data for studying maritime

tropospheric duct inversion from over-the-horizon, anomalously propagated ocean forward-scattered GPS L1 signals. In the experiment, a high-sensitivity delay-mapping receiver (located at 23.0282° N and 116.5571° E; Fig. 12) was used to collect and process direct and ocean-scattered GPS L1 signals. The antenna used to receive the scattered signal was left-hand circularly polarized (LHCP) and horizontally oriented toward the ocean surface with a high gain of 27 dB (Fig. 13, left). The meteorological parameters, including the temperature, humidity, and pressure of the atmosphere, were measured by 12 sensors mounted on a vertical tower (Fig. 13, right). These parameters were used to quantify the atmospheric conditions during the experiment, especially the modified refractivity. An overview of this experiment is given in Ref. [33].

We use the experimental data from three GPS satellites at an 8° elevation angle to validate the forward propagation model studied in the present work. In order to illustrate the variation of the received power resulting from satellite motion and sea state change, we draw all the power patterns recorded in the measuring period for each case, which are shown in Fig. 14. The larger dynamic range of the received power in Fig. 14(b) is due to a higher sea state in that measuring period. The experimental powers are received by the LHCP receiving antenna at a 5.6-m height above the mean sea level located in three

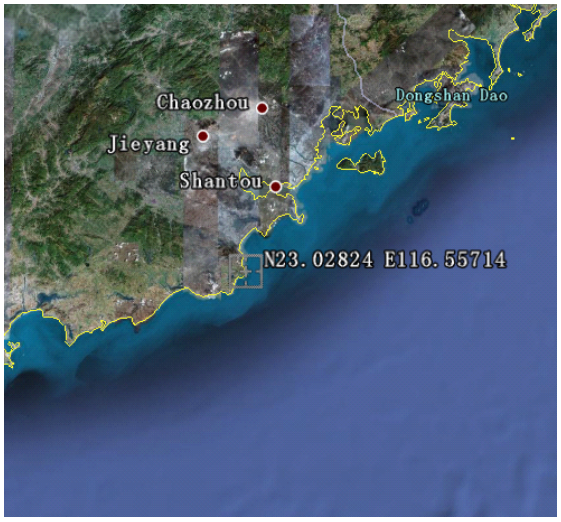


Fig. 12. (colour online) Location of the experiment.



Fig. 13. (colour online) (left) LHCP antenna for receiving the scattered GPS signal, and (right) 12 meteorological sensors mounted on a tower.

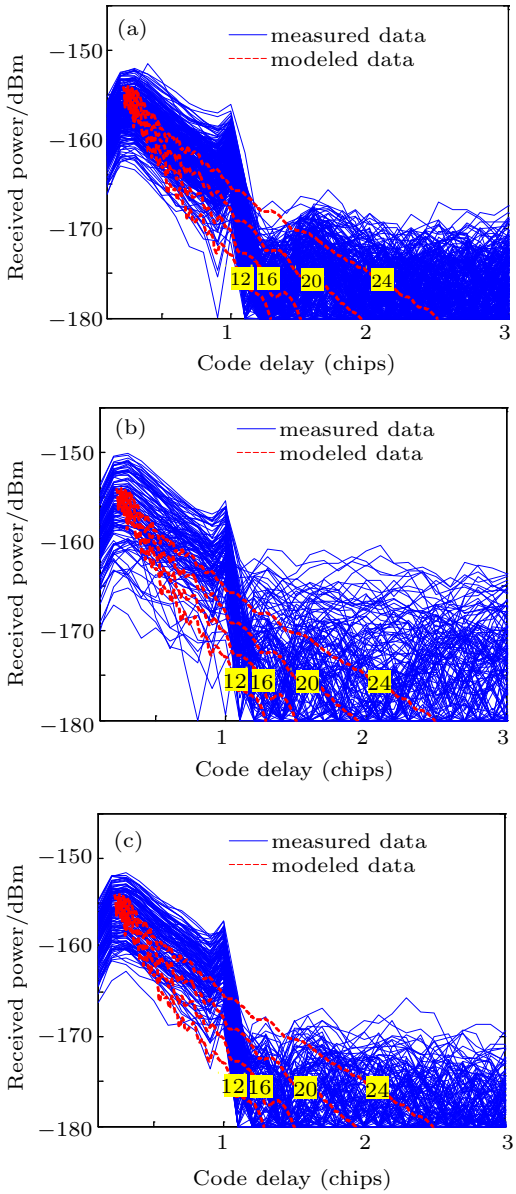


Fig. 14. (colour online) Measured (solid line) and modeled (dotted line) power of the ocean forward-scattered GPS signals. (a) Data from GPS PRN 15 at an 8° elevation angle recorded from 11:00:29 to 11:05:29 on June 13. (b) Data from GPS PRN 9 at an 8° elevation angle recorded from 12:15:58 to 12:18:09 on June 16. (c) Data from GPS PRN 12 at an 8° elevation angle recorded from 13:45:34 to 13:47:56 on June 16. The numbers on the gray background indicate the EDHs.

ducting environments shown in Fig. 15. The M-profiles are measured only by 12 meteorological sensors mounted on a vertical tower located at the seacoast; hence, the altitude resolution is low and information about range-dependent refractivity above the ocean surface cannot be obtained. These M-profiles cannot accurately describe the actual ducting environment, and they are therefore not used in generating the modeled power. We employ them only to qualitatively indicate the atmospheric environment. Because these roughly measured M-profiles indicate evaporation duct environments, four log–linear Paulus–Jeske M-profiles (EDH = 12, 16, 20, and 24 m) are used simultaneously for generating the received power patterns of the scattered GPS signals to match the measured power patterns.

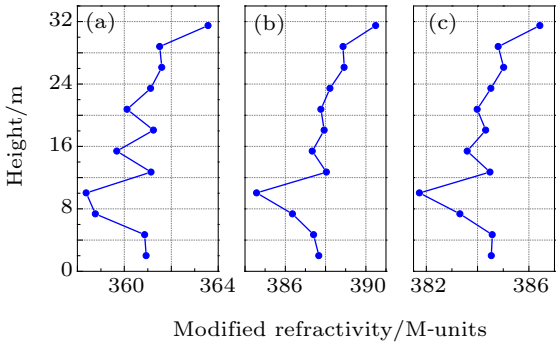


Fig. 15. Measured modified refractivity profiles. (a) Average of 29 profiles recorded from 11:00:29 to 11:05:29 on June 13. (b) Average of 27 profiles recorded from 12:15:58 to 12:18:09 on June 16. (c) Average of 28 profiles recorded from 13:45:34 to 13:47:56 on June 16.

Figure 14 shows that the four modeled power patterns match the measured data, with different fitting values. Determining which modeled power pattern has a better fit is a hard job because all the matches are rough. These rough matches are probably due to the rough calculation of the bistatic scattering coefficient of the ocean surface and the assumption of range-independent evaporation duct M-profiles, which cannot represent the refractivity field over a large ocean surface. Although these matches are rough, the trend in range (code delay) and magnitude of the modeled power level basically tally with those of the measured data. This result demonstrates that the propagation model in the present study can model the propagation of ocean forward-scattered low-elevation GPS signals within tropospheric ducts and serve as a forward model for duct inversion. For robust inversion, however, this model may need to be improved because high-precision inversion necessitates a good match between experimentally measured power and prediction from the forward model. In Fig. 14, the zero chip of the code delay corresponds to the specular, reflected GPS signal, for the 8° elevation angle and the 5.6-m height of the receiving antenna, and two chips approximately correspond to a value of 56 km of the range along the ocean surface.

6. Possibility of maritime tropospheric duct inversion from ocean-scattered GPS signals

Two conditions should be ensured to enable tropospheric duct inversion from the ocean forward-scattered low-elevation GPS signals. First, the ocean forward-scattered GPS signals must be affected significantly or trapped by the tropospheric duct. This requirement is satisfied according to the trapping capability analysis presented in Section 2. Second, these signals must carry abundant information about atmospheric refractivity before reaching the receiver. That is, the received power as a function of range of the scattered signals should have high sensitivity to the duct parameters (e.g., the EDH of the evaporation duct) because the inversions of the tropospheric duct (i.e., retrievals of duct parameters) are performed by matching the experimentally measured received power patterns against the predictions of the forward propagation model. If sensitivity is low, inversion will be difficult.

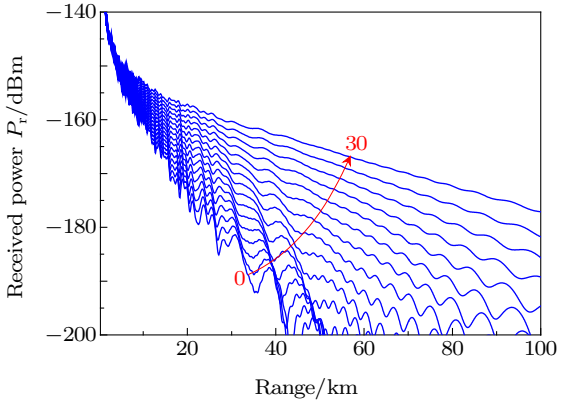


Fig. 16. Curves of received GPS scattered power versus range R_2 in the evaporation ducts with the EDH ranging from 0 to 30 m, in steps of 2 m. The arrow shows the evolution of the power pattern as EDH increases.

The sensitivity of the received power to the evaporation duct height is discussed as an example. We assume that the receiving antenna has the parameters given in Table 1 and the GPS elevation angle is 5°. The levels of received power of the ocean forward-scattered GPS signals for EDHs ranging from 0 to 30 m are shown in Fig. 16. The power strength increases monotonically as the EDH increases, and this behaviour is approximately linear. The power increment is approximately 2 dB at 50 km and 5 dB at 100 km. This power variation indicates an appropriate or sufficient sensitivity to EDH, which guarantees successful tropospheric duct inversion.

Successful and high-quality tropospheric duct inversion necessitates conditions other than power sensitivity to the EDH. For example, a high-sensitivity receiver is necessary for receiving the GPS signals scattered from areas of the ocean surface at large distances. An experimental power pattern for a long range interval yields a higher-quality inversion result. Furthermore, supplemental information such as regional statistics on occurrence rates and strengths of tropospheric ducts can be employed to improve the inversion algorithm performance.

7. Conclusions and future work

On the basis of the parabolic equation technique and bistatic radar equation theory, we develop a propagation model that predicts the trapped propagation characteristics of ocean forward-scattered low-elevation GPS signals in tropospheric duct environments. The propagation model is expected to be adopted as a forward model in inversion problems of inferring the maritime tropospheric ducts from ocean forward-scattered GPS signals. The power-versus-range data from these signals predicted by this model basically tally with the data obtained from a GPS scattered signal receiving experiment conducted in the South China Sea, which indicates that this propagation model can predict the long-range propagation of ocean forward-scattered GPS signals within tropospheric ducts, and can serve as a forward model for duct inversion.

Many factors can affect the fit between experimental power and predicted power. First, the bistatic scattering coefficient of the ocean surface which is used in the PWE initial field definition can significantly affect the strength of predicted power. Second, the modified refractivity profile is assumed to be uniform along the propagation path, which results in errors in the prediction on power. Furthermore, experimental power may be negatively affected by power from unexpected signals of many types, such as receiver thermal noise and the scattered GPS signals from ships. All these factors should be considered carefully in future work to improve the fitting between the two power patterns and the accuracy of the maritime tropospheric duct inversion.

References

[1] Hall M P M 1979 *Effects of the Troposphere on Radio Communication* (London: Peter Peregrinus)

[2] Turton J D, Bennetts D A and Farmer S F G 1988 *Meteorol. Mag.* **117** 245

[3] Rowland J R, Konstanzer G C, Neves M R, Miller R E, Meyer J H and Rottier J R 1996 *Proceedings of the Battlespace Atmospherics Conference,* December, 1996, San Diego, USA, p. 155

[4] Richter J H 1994 *Proceedings of the International Geoscience and Remote Sensing Symposium,* August 8–12, 1994. Pasadena, USA, p. 381

[5] Haack T and Burk S D 2001 *J. Appl. Meteorol.* **40** 673

[6] Kuttler J R and Dockery G D 1991 *Radio Sci.* **26** 381

[7] Levy M F 2000 *Parabolic Equation Methods for Electromagnetic Wave Propagation* (London: The Institution of Electrical Engineers)

[8] Rogers L T, Hattan C P and Stapleton J K 2000 *Radio Sci.* **35** 955

[9] Gerstoft P, Rogers L T, Krolik J L and Hodgkiss W S 2003 *Radio Sci.* **38** 8053

[10] Yardim C, Gerstoft P and Hodgkiss W S 2006 *IEEE Trans. Antennas Propag.* **54** 1318

[11] Huang S X, Zhao X F and Sheng Z 2009 *Chin. Phys.* B **18** 5084

[12] Zhao X F, Huang S X, Xiang J and Shi W L 2011 *Chin. Phys.* B **20** 099201

[13] Sheng Z and Huang S X 2010 *Acta Phys. Sin.* **59** 1734 (in Chinese)

[14] Zhao X F, Huang S X and Sheng Z 2010 *Chin. Phys.* B **19** 049201

[15] Zhao X F and Huang S X 2011 *Chin. Phys.* B **20** 029201

[16] Karimian A, Yardim C, Gerstoft P, Hodgkiss W S and Barrios A E 2011 *Radio Sci.* **46** RS6013

[17] Martín-Neira M 1993 *ESA Journal* **17** 331

[18] Garrison J L, Katzberg S J and Hill M I 1998 *Geophys. Res. Lett.* **25** 2257

[19] Lowe S T, Zuffada C, Chao Y, Kroger P, Young L E and LaBrecque J L 2002 *Geophys. Res. Lett.* **29** 1375

[20] Marchan-Hernandez J F, Valencia E, Rodriguez-Alvarez N, Ramos-Perez I, Bosch-Lluis X, Camps A, Eugenio F and Marcello J 2010 *IEEE Geosci. Remote Sens. Lett.* **7** 621

[21] Komjathy A, Zavorotny V U, Axelrad P, Born G H and Garrison J L 2000 *Remote Sens. Environ.* **73** 162

[22] Garrison J L, Komjathy A, Zavorotny V U and Katzberg S J 2002 *IEEE Trans. Geosci. Remote Sens.* **40** 50

[23] Anderson K D 1994 *Proceedings of AGARD Conference* **567** p. 1

[24] Lowry A R, Rocken C, Sokolovskiy S V and Anderson K D 2002 *Radio Sci.* **37** 1041

[25] Paulus R A 1990 *IEEE Trans. Antennas Propag.* **38** 1765

[26] Rogers L T 1997 *Radio Sci.* **32** 79

[27] Dockery G D and Kuttler J R 1996 *IEEE Trans. Antennas Propag.* **44** 1592

[28] Miller A R, Brown R M and Vegh E 1984 *IEE Proc. Microwaves Opt. Antennas* **131** 114

[29] Beckmann P and Spizzichino A 1987 *The Scattering of Electromagnetic Waves from Rough Surfaces* (Norwood: Artech House)

[30] Thorsos E I 1988 *J. Acoust. Soc. Am.* **83** 78

[31] Yang C, Guo L X and Wu Z S 2010 *Chin. Phys.* B **19** 054101

[32] Tsang L, Kong J A, Ding K H and Ao C O 2001 *Scattering of Electromagnetic Waves: Numerical Simulations* (New York: John Wiley & Sons, Inc.)

[33] Wang B, Wu Z S, Zhao Z W and Wang H G 2011 *IEEE Geosci. Remote Sens. Lett.* **8** 587